

Fabrication update on critical-angle transmission gratings for soft x-ray grating spectrometers

Ralf K. Heilmann, Alex Bruccoleri, Pran Mukherjee,
Jonathan Yam, and Mark L. Schattenburg,

Space Nanotechnology Laboratory, MIT Kavli Institute for Astrophysics and Space Research,
Massachusetts Institute of Technology, Cambridge, Massachusetts 02139, USA

ABSTRACT

Diffraction grating-based, wavelength dispersive high-resolution soft x-ray spectroscopy of celestial sources promises to reveal crucial data for the study of the Warm-Hot Intergalactic Medium, the Interstellar Medium, warm absorption and outflows in Active Galactic Nuclei, coronal emission from stars, and other areas of interest to the astrophysics community. Our recently developed critical-angle transmission (CAT) gratings combine the advantages of the Chandra high and medium energy transmission gratings (low mass, high tolerance of misalignments and figure errors, polarization insensitivity) with those of blazed reflection gratings (high broad band diffraction efficiency, high resolution through use of higher diffraction orders) such as the ones on XMM-Newton. Extensive instrument and system configuration studies have shown that a CAT grating-based spectrometer is an outstanding instrument capable of delivering resolving power on the order of 5,000 and high effective area, even with a telescope point-spread function on the order of many arc-seconds. We have fabricated freestanding, ultra-high aspect-ratio CAT grating bars from silicon-on-insulator wafers using both wet and dry etch processes. The 200 nm-period grating bars are supported by an integrated Level 1 support mesh, and a coarser external Level 2 support mesh. The resulting grating membrane is mounted to a frame, resulting in a grating facet. Many such facets comprise a grating array that provides light-weight coverage of large-area telescope apertures. Here we present fabrication results on the integration of CAT gratings and the different high-throughput support mesh levels and on membrane-frame bonding. We also summarize recent x-ray data analysis of 3 and 6 micron deep wet-etched CAT grating prototypes.

Keywords: x-ray optics, critical-angle transmission grating, x-ray spectroscopy, blazed transmission grating, soft x-ray, silicon-on-insulator, deep reactive-ion etching

1. INTRODUCTION

Even twelve years after launch, the Chandra X-ray Observatory still stands unchallenged in terms of the 0.5 arcsec point-spread function (PSF) of its imaging mirrors. In order to fully exploit this high imaging resolution for grating spectroscopy, Chandra was equipped with the High Energy Transmission Grating Spectrometer (HETG).¹ The transmission geometry is highly insensitive to grating alignment and figure errors and therefore translates sharp imaging resolution into equally sharp spectral resolution. The same would not have been possible with reflection gratings that would have degraded the spectrometer resolving power due to their own figure errors. The Reflection Grating Spectrometer (RGS)² aboard XMM-Newton could tolerate ~ 3 arcsec reflection grating figure and alignment errors, since the imaging PSF alone already exceeded 10 arcsec. However, the HETG efficiency is limited by grating absorption, and its resolving power is limited by the dispersion of its 200 nm-period gratings, since most x rays are detected in first order. Blazing, which is often implemented with reflection gratings, enables channeling of diffracted power for shorter wavelengths into higher diffraction orders and therefore leads to higher resolving power. Efficient blazing over a broad wavelength band is best achieved for soft x rays via reflection at small angles of grazing incidence, below the critical angle for total external reflection. Grazing incidence reflection also minimizes absorption, since x rays mostly traverse vacuum. We therefore set out to combine the advantages of both transmission and reflection gratings, resulting in the critical-angle transmission (CAT) grating geometry shown in Fig. 1.

Further author information: Send correspondence to R.K.H. E-mail: ralf@space.mit.edu, URL: <http://snl.mit.edu/home/ralf>

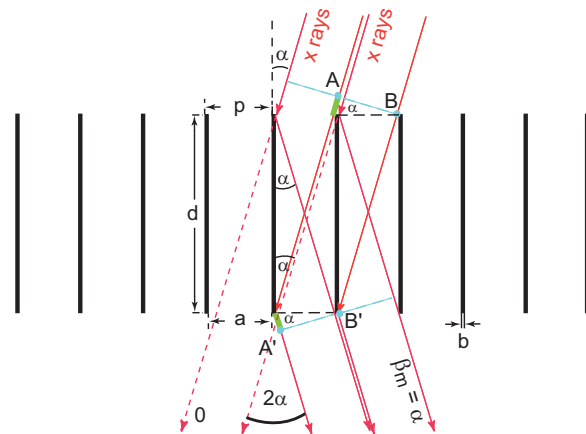


Figure 1. Schematic cross section through a CAT grating. The m^{th} diffraction order occurs at an angle β_m where the path length difference between AA' and BB' is $m\lambda$. Shown is the case where β_m coincides with the direction of specular reflection from the grating bar side walls ($\beta_m = \alpha$), i.e., blazing in the m^{th} order.

X rays are incident onto the thin, ultra-high aspect-ratio grating bar side walls at an angle α below the critical angle for total external reflection, θ_c . Every x ray incident upon the space between grating bars undergoes a single reflection. The optimum grating depth d is $d = a/\tan \alpha$, where a is the space between two adjacent grating bars. The grating bar thickness b should be small in order to minimize absorption or blockage of x rays. The grating bar side walls need to be nm-smooth or better to minimize scattering losses. For soft x rays θ_c is typically on the order of $1 - 5^\circ$.

The grating equation describes the relationship between the angle β_m at which the m^{th} diffracted order is observed, the wavelength λ of the light incident at angle α , and the grating period p ,

$$\frac{m\lambda}{p} = \sin \alpha - \sin \beta_m, \quad (1)$$

with $m = 0, \pm 1, \pm 2, \dots$. We have fabricated CAT grating prototypes with periods of 574^{3-5} and $200 \text{ nm}^{4,6-9}$ with anisotropic wet etching of lithographically patterned $\langle 110 \rangle$ silicon-on-insulator (SOI) wafers in potassium hydroxide (KOH) solutions. We have achieved small grating bar duty cycles ($b/p < 20\%$) and unprecedented grating bar aspect ratios (d/b up to 150), as well as smooth side walls. X-ray tests have shown that our grating prototypes perform at the level of 50-100% of theoretical predictions for ideal CAT gratings over a broad wavelength band.^{5,9}

Over the last few years we have performed extensive configuration, design and ray-trace studies for a critical-angle transmission grating spectrometer (CATGS)^{4,7,8,10} for the International X-ray Observatory (IXO).¹¹ The IXO follows the basic concept of an imaging telescope with Wolter I focusing mirrors and imaging instruments at focus. The CATGS is comprised of one or more CAT grating arrays at maximum distance from focus, and a linear CCD readout array that extends in the radial direction from the telescope focus, detecting the diffracted spectrum within the grating blaze envelope. We have demonstrated that a lightweight CATGS is capable of delivering spectral resolving power on the order of $\lambda/\Delta\lambda \sim 5000$, even with a 5 arcsec telescope imaging PSF and relaxed alignment tolerances. The CATGS also promises high effective area due to the high CAT grating diffraction efficiency ($\sim 5\times$ the efficiency of the Chandra high and medium energy gratings for soft x rays) and minimal area losses from a hierarchy of support structures that hold the freestanding grating bars in place. In addition, CAT gratings become highly transparent at higher energies, so that effective area losses for an imaging detector at the telescope focus are minimized for short-wavelength x rays. Of course the CATGS concept can be readily adapted to future x-ray telescopes that might replace IXO, such as the ATHENA (Advanced Telescope for High ENergy Astrophysics) mission currently under study at ESA.

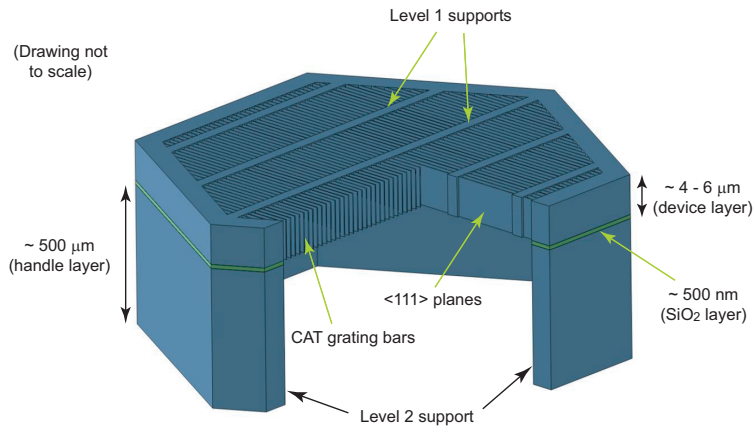


Figure 2. Schematic of a grating membrane “unit cell” (not to scale), formed by a L2 support mesh hexagon. The L2 mesh is etched out of the SOI handle layer (backside). The device layer contains the fine-period CAT grating bars and in the perpendicular direction the coarse, low duty cycle integrated L1 support mesh. Device and handle layers are separated by the thin buried silicon oxide layer that serves as an etch stop for both front and back side etches.

We are currently focusing on increasing the Technology Readiness Level (TRL) for CAT gratings. Our past successful x-ray tests on wet-etched prototypes put CAT grating technology at TRL 3. However, the anisotropic nature of the KOH etch depends on the lattice plane orientation within the single-crystal SOI device layer. The etch mask for this layer contains the CAT grating bar pattern and the pattern for a coarse Level 1 (L1) support mesh. While the CAT grating bars etch along vertical $\langle 111 \rangle$ silicon crystal planes, the support mesh bars protect slanted $\langle 111 \rangle$ planes from being etched. This leads to a trapezoidal broadening of the support mesh bars with increasing etch depth and robs area from the CAT grating bars. We have achieved $\sim 45\%$ CAT grating area on $3.2 \mu\text{m}$ deep, 200 nm -period gratings, with the other 55% of the area blocked by the support mesh with periods on the order of tens of microns, but our goal is $80 - 90\%$ open area for CAT grating bars. However, the support mesh bars can not be spaced too far from each other, or else the long span that the CAT grating bars need to bridge can lead to grating bar collapse. The wet-etch fabrication approach is therefore limited in the achievable open area, and we have turned to plasma-based (“dry”) deep-etch processes since that will allow us to simultaneously etch CAT grating and support mesh bars vertically into the SOI device layer.

Another aspect of increased TRL is the size or area of the gratings themselves. The SOI device layer (“front side”) has the same thickness as the desired grating depth d . The freestanding CAT grating layer with its integrated L1 support mesh will form a thin (a few microns), perforated silicon membrane. This membrane should extend over $\sim 10 - 20 \text{ cm}^2$ to keep the number of gratings in an array reasonably small. A membrane so thin with such a large area needs additional structural support to survive the mechanical stresses of launch. These so-called Level 2 (L2) supports can be etched out of the $\sim 0.5 \text{ mm}$ thick handle layer (“back side”) of the SOI wafer. This is a fairly standard process by itself, but the challenge is to integrate this back side process with the much more sensitive front side process. Fig. 2 shows a schematic of a membrane “unit cell” defined by a single L2 support hexagon.

Finally, we must be able to integrate many grating membranes into a grating array. The SOI structure does not lend itself to direct mechanical precision mounting to a grating array structure (GAS). We therefore mount a grating membrane to a metal or ceramic frame, which in turn can then be mounted to a GAS. We refer to the union of a grating membrane and its frame as a grating facet.

2. X-RAY DIFFRACTION EFFICIENCY OF WET-ETCHED CAT GRATING PROTOTYPES

We had previously presented x-ray diffraction efficiency results from a large period CAT grating prototype,⁵ and preliminary analysis of x-ray measurements on 200 nm -period samples.⁷ Recently we have performed a more

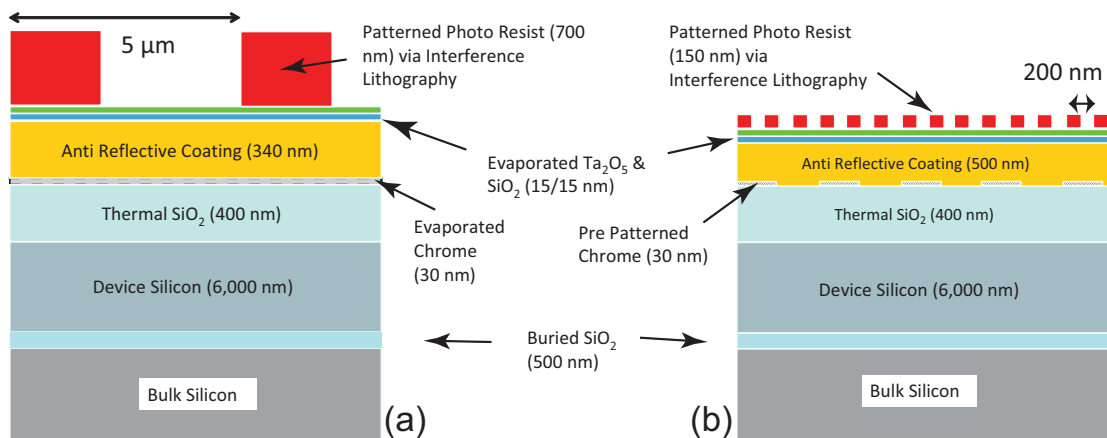


Figure 3. Layer stacks for an integrated chrome/ARC mask that leads to a single-layer thermal oxide mask for the simultaneous etching of CAT grating bars and L1 supports. See text for details.

detailed analysis of x-ray data from 3.2 and 6 μm deep wet-etched samples.⁹ This analysis explicitly takes into account the shape of the trapezoidal support mesh bars and the resulting wide range of depths and widths of the CAT grating bars that are concurrently present in a single sample. We found the expected blazing and diffraction efficiency at essentially 100% of theoretical predictions for a perfect CAT grating at $\lambda > 3.5 - 5$ nm. Towards shorter wavelengths performance slowly falls to as low as 50% of theory, which could be due in part to structural weakness from the large span between support mesh bars which may facilitate grating bar deformations.

3. DRY ETCH FABRICATION OF ULTRA-HIGH ASPECT RATIO CAT GRATINGS WITH INTEGRATED L1 SUPPORT MESH

Deep reactive-ion etching (DRIE) of silicon is a widespread technique for the highly anisotropic etching of silicon. In the Bosch DRIE process a nearly isotropic plasma etch step is repeatedly alternated with a passivation step. The resulting notorious scalloping of the etch trench side walls can be ameliorated by going to shorter etch/passivation cycles. Nevertheless, DRIE has rarely been used for the combination of small features and high aspect-ratios required for CAT gratings. Due to the limited DRIE selectivity between silicon oxide and silicon we first had to develop a high-aspect ratio oxide hard mask.¹² With this more than 400 nm deep oxide mask we have repeatedly etched 200 nm-period gratings up to 6 μm deep into bulk silicon.¹² We have since also performed this etch for CAT gratings with an integrated 5 μm -period, low duty cycle support mesh on SOI wafers and successfully stopped on the buried oxide layer. Unfortunately, we are severely limited in our DRIE process development since for the deepest etches we have to rely on a shared modern STS Pegasus tool at the University of Michigan to which we have limited access. In order to move development forward we have decided for now to work in parallel with 4 μm thick SOI device layers, which provide better process yield. This CAT grating depth is sufficient for many soft x-ray spectroscopy applications in astronomy, and together with future modifications (such as atomic layer deposition of high-Z metals onto CAT grating bars) it can even meet all aspects of the IXO CATGS science case.

Fig. 3(a) shows the layer stack for the L1 support mesh. Processing of the stack leads to a thin chrome mesh pattern on top of the thermal silicon oxide layer. The stack shown in Fig. 3(b) is added to the chrome mask to create a 200 nm-period CAT grating mask from the anti-reflective coating (ARC) layer in the direction perpendicular to the support mesh lines. Chrome and ARC then serve as a mask for the etch of the thermal oxide layer, which in turn becomes the integrated CAT grating/L1 support mask for the DRIE of the SOI device layer. An example of a thermal oxide mask for the deep silicon etch is shown in Fig. 4(a). Fig. 4(b) and (c) show some deep etching results that transfer the integrated oxide mask pattern into the silicon layer. The vertical support mesh side walls show that with DRIE we can easily obtain $> 80\%$ open area for a CAT grating.

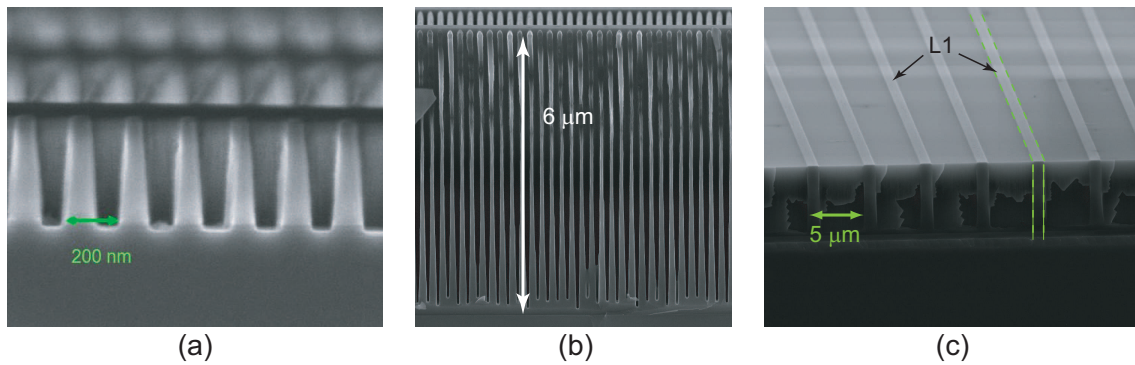


Figure 4. Scanning electron micrographs (SEM) of CAT grating fabrication with integrated L1 mesh. (a) Cleaved cross section of a thermal silicon oxide mask on top of silicon. (b) Cross section after a 6 micron DRIE into silicon. (c) Cross section of the same sample after DRIE, cleaved in the direction perpendicular to the L1 supports. One L1 mesh bar is highlighted with dashed lines, showing no detectable widening of the bar with increasing etch depth.

4. FABRICATION OF LEVEL 2 SUPPORT MESH

The L2 support mesh is etched out of the handle layer of the SOI wafer (typical thickness $\sim 500 \mu\text{m}$). The goal of the L2 mesh is to provide mechanical support to the device layer membrane that holds the CAT grating with its L1 mesh. The L2 mesh effectively divides a large device layer membrane into many small membranes with higher resonant frequencies, and it provides overall stiffness due to its considerable thickness. At the same time the L2 mesh should have minimal impact on the open area of the CAT gratings. We are currently experimenting with L2 mesh duty cycles in the range of $\sim 5 - 25\%$. So far, mechanical strength does not seem to be a problem even for the smallest duty cycles. Through-wafer DRIE of structures similar to the L2 mesh is relatively straightforward on bulk silicon wafers, and we have produced a number of L2 mesh samples with various sizes, geometries, and duty cycles.

5. INTEGRATION OF FRONT AND BACK SIDE PROCESSING

Integration of processing of both sides of an SOI wafer for large area CAT grating membrane is challenging. DRIE has to be done on both sides, and both etches have to stop on a thin ($0.5 \mu\text{m}$) buried oxide (BOX) layer that serves as an etch stop. The BOX layer has compressive stress that has the potential to distort the device layer. Thinner BOX layers lead to less distortion, but also limit the amount of allowed overetching for the DRIE before breaking through the etch stop. Samples have to be mounted to carrier wafers for DRIE on one side without damaging masks and structures that have already been fabricated on the other side. Which side is better to process first is up for discussion. We have experimented with back side etching first, but it appears that once the BOX layer is freed from the thick handle layer it buckles under compressive stress, which leads to complications during subsequent front side DRIE. Our work is currently focused on etching the front side first. After DRIE on the front side the device layer is then covered by photoresist for protection, and the sample is bonded to a carrier wafer with the device layer side facing the carrier. We then perform back side DRIE, stop on the BOX, debond the sample, and clean the resist off the front. The BOX layer is removed with hydrofluoric acid.

Fig. 5 shows images of a recently fabricated sample with freestanding CAT gratings and two levels of support structures. As seen in Fig. 6, the etch steps created the desired structures, but the CAT gratings were damaged at some point during the wet debonding and cleaning processes or the subsequent drying in air. Critical point drying³ was not used on this sample, which may be the main reason for the observed grating damage.

DRIE of front and back sides is working fairly well. On large-area samples we see evidence for loading effects (etch rate variations due to locally varying pattern densities) that can lead to slow L2 pattern duty cycle variations from the center of the hexagon array towards the edge. Repeatable duty cycle variations can

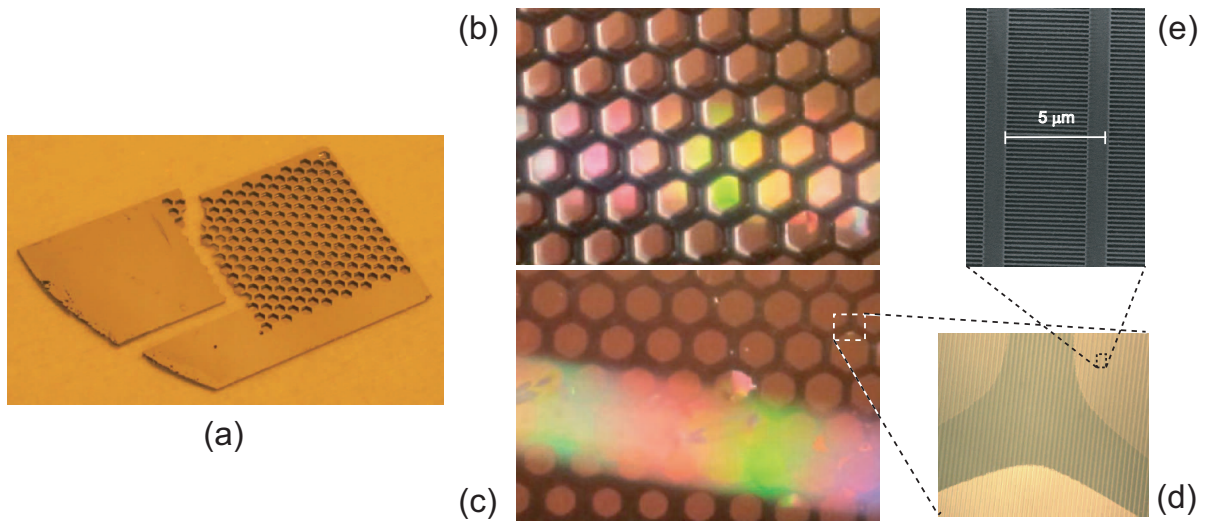


Figure 5. Examples of front and back side etched, large area gratings with two levels of support structures. (a) Backside view of a recent sample that was accidentally dropped on the floor. Most device layer membranes on the front side covering the L2-hexagons survived unharmed, attesting to the relative ruggedness of the structure. The hexagons cover an area of $\sim 6 \text{ cm}^2$. (b) Closeup view of the same sample from the back, showing the deep, low-duty cycle L2-hexagons in detail. The varying colors are due to diffraction from the L1 supports in the device layer. The hexagon period is close to 1.9 mm. (c) Front side view of the same sample. The translucent $4 \mu\text{m}$ device layer is illuminated from the back, making the handle layer L2-hexagons visible. Again the color bands are due to diffraction from the L1 supports. (d) Optical microscope image of a different back-illuminated sample before front side DRIE, showing the oxide mask for the L1 supports, with the already etched L2 supports casting a shadow. (e) Top-down SEM of the same sample as in (d), showing the oxide mask for the integrated L1 and CAT grating pattern.

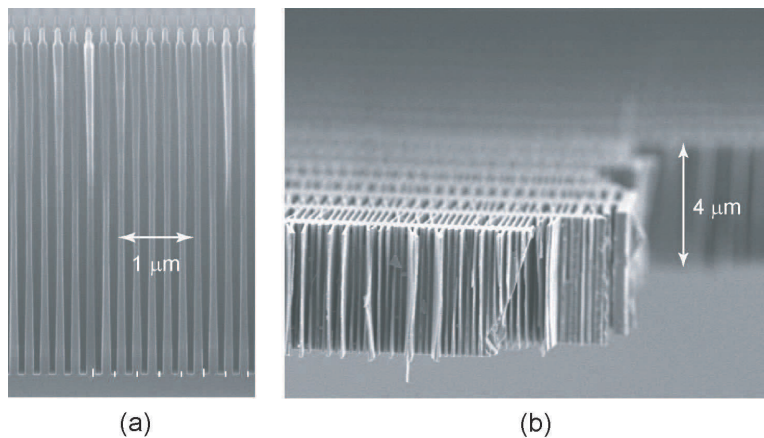


Figure 6. SEMs of fabrication results. (a) Cleaved cross section of a front side DRIE, stopping cleanly on the BOX layer (before back side processing). (b) View of the edge of a broken membrane (after back side processing), showing the freestanding CAT grating bars with the integrated L1 support mesh. Numerous CAT grating bars show stiction,³ probably due to lack of critical point drying.

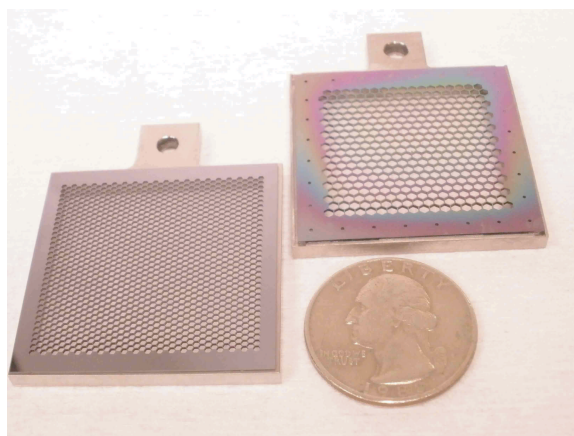


Figure 7. Two $38 \times 38 \text{ mm}^2$ Invar facet frames with L2 support mesh silicon membranes. The membranes have different hexagon sizes, and their L2 duty cycles are 10% (left facet) and 12.5% (right facet), respectively.

be reduced through bias in future mask patterns. The main issue to be addressed at the moment is a reliable method to protect and clean the etched CAT grating before and after back side DRIE.

6. INTEGRATION OF GRATING MEMBRANE AND EXTERNAL FRAME

We have also begun to investigate approaches toward the bonding of a grating membrane to an external flight frame, and to study the mechanical properties of the resulting grating facet. Since the elastic and mechanical properties of the grating membrane are dominated by the L2 mesh, we are initially using samples that only have L2 supports and are through-etched from a bulk silicon wafer instead of complete CAT grating membranes. As frame materials we are considering Invar, H-Invar, Hexoloy®SA silicon carbide, etc. Example candidates for bonding agents are low thermal expansion, low outgassing epoxies and reactive bonding. Fig. 7 shows some of our first test objects that will undergo vibration and thermal testing. We shall use finite-element modeling to analyze test results and to optimize frame and membrane structures for minimum mass and maximum open area.

7. DISCUSSION, SUMMARY, AND OUTLOOK

After having experimentally demonstrated the CAT grating principle with small wet-etched, low open-area-fraction prototypes, we are now well on our way towards fabrication of large-area, high open-area-fraction dry-etched CAT grating membranes that contain the full structural complexity required for TRL 4-6. The remaining steps are to find a reliable process for front side protection and cleaning, as well as a short KOH polish. The polish is probably required since we do not expect the dry-etched CAT grating bar side walls to be smooth enough for efficient blazing. Polishing with KOH will also necessitate accurate alignment of the CAT grating pattern to the crystal planes in the SOI handle layer similar to our previous work.^{3,6} Our progress has been slowed by lack of convenient access to a state-of-the-art DRIE tool. The progress we have made was only possible remotely with a tool at the University of Michigan. Nevertheless, we expect to be able to move forward towards large, highly efficient CAT gratings ready for integration into a high-resolution transmission grating spectrometer.

ACKNOWLEDGMENTS

We gratefully acknowledge technical support from F. DiPiazza (Silicon Resources) and facilities support from the Nanostructures Laboratory and the Microsystems Technology Laboratories (both at MIT). This work was performed in part at the Lurie Nanofabrication Facility, a member of the National Nanotechnology Infrastructure Network, which is supported by the National Science Foundation. This work was supported by NASA grants NNX08AI62G and NNX11AF30G.

REFERENCES

- [1] C. R. Canizares *et al.*, "The Chandra high-energy transmission grating: Design, fabrication, ground calibration, and 5 years in flight," *PASP* **117**, 1144-1171 (2005).
- [2] J. W. den Herder *et al.*, "The reflection grating spectrometer on board XMM-Newton," *Astr. & Astroph.* **365**, L7-L17 (2001).
- [3] M. Ahn, R. K. Heilmann, and M. L. Schattenburg, "Fabrication of ultrahigh aspect ratio freestanding gratings on silicon-on-insulator wafers," *J. Vac. Sci. Technol. B* **25**, 2593-2597 (2007).
- [4] R. K. Heilmann, M. Ahn, and M. L. Schattenburg, "Fabrication and performance of blazed transmission gratings for x-ray astronomy," *Proc. SPIE* **7011**, 701106 (2008).
- [5] R. K. Heilmann, M. Ahn, E. M. Gullikson, and M. L. Schattenburg, "Blazed high-efficiency x-ray diffraction via transmission through arrays of nanometer-scale mirrors," *Opt. Express* **16**, 8658-8669 (2008).
- [6] M. Ahn, R. K. Heilmann, and M. L. Schattenburg, "Fabrication of 200 nm-period blazed transmission gratings on silicon-on-insulator wafers," *J. Vac. Sci. Technol. B* **26**, 2179-2182 (2008).
- [7] R. K. Heilmann *et al.*, "Development of a critical-angle transmission grating spectrometer for the International X-Ray Observatory," *Proc. SPIE* **7437**, 74370G (2009).
- [8] R. K. Heilmann *et al.*, "Critical-angle transmission grating spectrometer for high-resolution soft x-ray spectroscopy on the International X-Ray Observatory," *Proc. SPIE* **7732**, 77321J (2010).
- [9] R. K. Heilmann, M. Ahn, A. Bruccoleri, C.-H. Chang, E. M. Gullikson, P. Mukherjee, and M. L. Schattenburg, "Diffraction efficiency of 200 nm period critical-angle transmission gratings in the soft x-ray and extreme ultraviolet wavelength bands," *Appl. Opt.* **50**, 1364-1373 (2011).
- [10] K. Flanagan *et al.*, "Spectrometer concept and design for x-ray astronomy using a blazed transmission grating," *Proc. SPIE* **6688**, 66880Y (2007).
- [11] J. Bookbinder, "An overview of the IXO Observatory," *Proc. SPIE* **7732**, 77321B (2010).
- [12] P. Mukherjee, A. Bruccoleri, R. K. Heilmann, M. L. Schattenburg, A. F. Kaplan, and L. J. Guo, "Plasma etch fabrication of 60:1 aspect ratio silicon nanogratings on 200 nm pitch," *J. Vac. Sci. Technol. B* **28**, C6P70-5 (2010).